Removal of cesium and strontium ions with enhanced solid-liquid separation by combined ion exchange and BaSO₄ co-precipitation

Oguzhan Kivan [a,*], Muhammad Yusuf [a,b], David Harbottle [a], Timothy N. Hunter [a,*]

[a] School of Chemical and Process Engineering, University of Leeds, Leeds LS2 9JT, UK
[b] Research Center for Nuclear Materials and Radioactive Waste Technologies (PRTBNLR), Research Organization for Nuclear Energy (ORTN), National Research and Innovation Agency (BRIN), South Tangerang 15314, Indonesia

ARTICLE INFO

ABSTRACT

Treatment of cesium and strontium is critical in radioactive liquid waste management, where their ions are difficult to remove in single operations, owing to differences in valence state. Here, the efficacy of composite coagulants synthesised by combining fine clinoptilolite with co-precipitated barite (BaSO₄) were investigated for the simultaneous removal of Cs^+ and Sr^{2+} ions, producing aggregates with enhanced dewatering properties. Co-precipitated BaSO₄ without clinoptilolite was found to be very effective in the removal of Sr^{2+} (>99 %) while only giving low-level Cs^+ removal (~14 %) for solutions containing 25 ppm of Cs^+ and Sr^2. Conversely, pure clinoptilolite gave high Cs^+ removal (>98 %) with rapid adsorption (<1 h) fitted to a Pseudo-Second Order (PSO) rate model. Composite coagulants were then produced using natural clinoptilolite combined with BaSO₄ co-precipitation. Higher Sr^{2+} removal was obtained in all cases (>99.9 %), whereas Cs^+ removal was reduced to <90 %, owing to exchange interactions with free Ba^{2+} ions. However, NaCl-preactivated clinoptilolite overcame low Cs^+ removal efficiency, achieving >95 % removal. Their physical properties, sedimentation rates, and compressional yield stress were also studied to characterise the aggregates solid-liquid separation behaviour. The combined coagulates obtained settling rates almost twice that of pure BaSO₄, and produced much greater consolidation, owing to increased aggregate density. Also, the combined systems had a higher gel point and lower specific compressive yield stress, suggesting less resistance to compression under centrifugal forces for dewatering. Overall, this study highlights that the use of composite coagulants can improve the removal efficiency of Cs^+ and Sr^{2+} while also accelerating solid-liquid dewatering.

1. Introduction

Radioactive wastewater containing fission products with different radioactivity and toxicity levels is generated through various activities. In particular, ^{137}Cs and ^{90}Sr ions are predominant concerns in spent fuel effluents, owing to their high radioactivity, relatively long half-life (30.17 years for ^{137}Cs and 28.8 years for ^{90}Sr), bioaccumulation tendency, and heat generation increasing the burden in waste management [1,2]. Specifically, ^{137}Cs is a high-yield fission product of uranium fuel that emits strong beta-gamma radiation and is responsible for the bulk radiation in waste solutions because of its high solubility, and for biological hazards in virtue of chemical similarities of potassium and sodium [3–5]. Likewise, ^{90}Sr is the other major contributor to radioactivity in spent fuel, emitting pure beta radiation and it gives rise to high radiological hazards, as it possesses relatively high solubility and

chemically acts similar to calcium [6,7]. Once introduced into the environment, their high mobility throughout ecosystems can cause organisms to absorb them, eventually reaching the human diet and inducing serious health effects, including cancer [8]. Since drinking water is a significant contamination pathway for humans, maximum allowable levels of ^{137}Cs and ^{90}Sr in drinking water are set by the Environmental Protection Agency (EPA) as 7.4 Bq/L for ^{137}Cs and 0.3 Bq/L for ^{90}Sr and the World Health Organization (WHO) as 10 Bq/L for both radionuclides [9–11]. However, routine nuclear-based activities, such as site water treatment or decommissioning, may increase the concentrations of ^{137}Cs and ^{90}Sr in the surface and groundwater [12,13]. Therefore, the efficient removal of these ions from waste solutions is critical for nuclear waste management and radiological protection strategy.

Extraction of ^{137}Cs and ^{90}Sr is challenging and requires well-suited

techniques following their nature in the solution. Studies have proven that conventional water treatment techniques, such as coagulation/flocculation plants, have low removal efficiencies, leading to the development of new efficient techniques [14,15]. Up to now, there are several methods employed to treat radioactive Cs^+ and Sr^{2+} ions based on the waste composition: namely, adsorption, ion exchange, chemical precipitation, evaporation, solvent extraction, membrane technologies, and electrochemical and biological methods [16–24]. Among them, physicochemical methods such as adsorption/ion exchange and chemical precipitation are perhaps the most widely studied and practiced techniques for low to intermediate-level radioactive waste streams [8]. However, many current methods suffer from poor sensitivity to harsh environmental conditions (i.e., radiation or chemical), high operating cost and energy demand, as well as low efficiency from completing ions in waste solutions [25,26].

In terms of adsorption/ion exchange materials, the natural zeolite clinoptilolite is a well-studied ion exchanger that is capable of removing Cs^+ and Sr^{2+} ions (to a degree) from waste solutions [27]. Due to superb resistance to radiation, being an appropriate material for column operation and encapsulation for final storage, it has been practically used in operations to purify water from various nuclear facilities, such as the Site Ion Exchange Effluent Plant) (SIXEP) at Sellafield, U.K. (Europe's largest legacy nuclear reprocessing facility) [18,28]. However, it is noted that clinoptilolite has been found to significantly more Cs^+ than Sr^{2+} in regular operations, and up to 20 times more moles of Cs^+ ions than Sr^{2+} in the presence of other matrix components such as Na^+, Mg^{2+}, and Ca^{2+}, and >2 times more [29]. The ideal pore diameters of clinoptilolite between 3.5 and 3.9 Å are most probably the main reason for the high affinity to the hydrated cesium ion sized ~3.45 Å [30]. Also, its leaching potential in harsh pH conditions and its sensitivity to high ionic strength, as well as competing ions, influence the removal efficiency of both ions [31,32].

Chemical (co)precipitation is another very common treatment technique for radioactive wastewater because of its flexibility in application, cost efficiency, and its effectiveness for large volumes of water containing high salt concentrations [33–35]. Chemical co-precipitation of Sr^{2+} can readily occur as carbonate, phosphate, nitrate, and sulphate compounds for pre-concentration or elemental separation purposes [36]. However, as Cs^+ salts have high solubility in water like other alkali metals, the chemical precipitation of Cs^+ is more difficult and limited with a couple of precipitating agents such as tetraphenylborate, hexacyanoferrates or ammonium phosphomolybdate [37–40]. One of the critical problems with chemical precipitation is the formation of colloidal and very fine-sized precipitates, which leads to a slow settling rate and increases the workload and cost of dewatering [41]. Additionally, the relatively high levels of co-precipitate chemicals required to form the main crystal material may lead to correspondingly large waste volumes. This issue makes the separation of solid precipitates from the liquid phase quite problematic and often requires additional integrated techniques such as membrane filtration or centrifugation [35,41]. Therefore, the formation of a denser particle with a suitable precipitate is important for easy and efficient solid-liquid separation.

Co-precipitation is widely used in ongoing operations, such as at Fukushima [42] or in the reprocessing plant at La Hague in France [43], where separate precipitation steps are used to remove both Cs^+ and Sr^{2+} ions by an appropriate solid carrier formed in situ, being metal hexacyanoferrates and barium sulphate (also known as barite, $BaSO_4$), respectively [44,45]. The co-precipitation with barite, in particular, is a well-adopted and implemented method to effectively remove Sr^{2+} ions from the wastewater along with other dangerous divalent ions e.g. ^{226}Ra or ^{210}Pb [46]. Additionally, barite is a well-studied and proven host material for co-precipitation providing superior advantages such as having very low solubility ($K_{sp} = 10^{-9.98}$), high crystal stability to harsh conditions, large ionic radii, and high density (4.5 g/cm^3) [43]. The lower solubility of $BaSO_4$ compared to its endmember $SrSO_4$, known as celestine, ($K_{sp} = 10^{-6.47}$), plays an important role in Sr^{2+} incorporation,

which means that Sr^{2+} co-precipitation can occur even in Sr-poor, unsaturated solutions [47,48].

Thus, in general, separate operations are required to remove Cs^+ and Sr^{2+} ions, where often a mixture of co-precipitation and ion exchange operations are employed. Also, the production of fine colloidal material and high waste volumes reduces the innate flexibility and simplicity of co-precipitation treatments, which increases the cost and workload due to the requirement for an efficient separation process, especially for Cs^+ removal [19]. However, it may be possible to combine both methods into a single process to produce composite aggregates with enhanced waste compaction and greater selectivity. Previous work has shown, for example, that fine mineral adsorbate materials can be added to hydroxide precipitation to enhance dye removal and accelerate sedimentation of produced sludges [49]. Another example has shown that adding activated carbon as an adsorbent to aluminium chloride precipitation can also improve the reactive dye removal efficiency and reduce the sludge volume [50]. Combined coagulation and adsorption have also been studied to control fouling in ultra-filtration membranes compared to single adsorption or coagulation, and the coagulation-adsorption process has been indicated to be effective in improving membrane fouling [51]. Up to now, far too little attention has been paid to the combined adsorption-coagulation process for the treatment of radioactive effluent, although, a recent study attempted to remove radioactive Cs^+ from a highly acidic solution using coagulation and adsorption steps and achieved a high removal of Cs^+ ions [52]. However, here, magnetic separation rather than sedimentation played an important role due to the coagulant type and small floc size [52]. Nevertheless, there is a lack of studies on combined adsorption-coagulation processes for the simultaneous removal of Cs^+ and Sr^{2+} ions, and related research into methods to significantly improve radioactive sludge dewatering allowing volume reduction for waste encapsulation.

Therefore, in this study, we investigate combined adsorption and co-precipitation methods to produce composite coagulants for enhanced solid-liquid dewatering. Taking advantage of the proven adsorption affinity of Cs^+ to clinoptilolite and the favourable crystal structure of $BaSO_4$ for rapid Sr^{2+} precipitation, fine clinoptilolite powder was added along with secondary $BaSO_4$ precipitation to generate core-sell aggregates promoting simultaneous Cs^+/Sr^{2+} along with enlarged structures for rapid separation. The synthesised composite particles were fully characterised, allowing an in-depth understanding of their structure and composition. In addition, the adsorption kinetics for clinoptilolite were studied in terms of the adsorption rate and condition using Cs^+ and Sr^{2+} ions together in the same solution. Moreover, the analytical sedimentation rates and profiles were then measured using centrifugal and gravitational force for the physical separation degree of suspension. Finally, compressional yield stress was analysed to study whether the suspension ben can easily be consolidated.

2. Materials and methods

2.1. Materials

Cesium nitrate ($CsNO_3$) and strontium nitrate ($Sr(NO_3)_2$) were of analytical grade with purity ≥99 % (Fluorochem Ltd., UK) and were used without any purification. Barium nitrate ($Ba(NO_3)_2$) and sodium sulphate ($NaSO_4$) were also purchased from Fluorochem Ltd. UK and used as received. The ion exchange utilised in combined studies was fine, milled clinoptilolite (Product Code: S25114, Fluorochem Ltd., UK) with a mean size of ±7 μm, as used previously for Cs^+ removal [53]. Analytical grade sodium chloride (NaCl) with purity ≥99 % (Fisher Scientific, UK) was used for clinoptilolite activation. Salt solutions and clinoptilolite dispersions were all produced in ultrapure deionised Milli-Q™ water (Millipore, USA).

2.2. Batch co-precipitation study

In the nuclear industry, high concentrations of barium sulphate (2–20 g/L) are generally made by mixing dissolved sodium sulphate and barium nitrate or barium chloride and used to treat radioactive waste solution containing radioactive strontium isotopes (i.e. ^{90}Sr) [54]. Therefore, an initial experiment was performed to synthesise barium sulphate particles without contaminants and to characterise the dispersions to ensure a clear understanding of BaSO$_4$ formation. As a next step, 25 mg/L of each SrNO$_3$ and CsNO$_3$ were added into the effluent solution together to study removal efficiency and to understand whether contaminant inclusion altered the physicochemical properties of the crystals. It is noted that during all experiments, non-radioactive cesium and strontium were used since stable isotopes have similar characteristics to their radioactive counterparts [55].

The initial batch experiment was based on the work of Pacary et al. [54] with some alterations. Here, ~2.5 wt% of BaSO$_4$ (barite) was synthesised at 25 °C with a mixture of 100 mL simulated effluent containing 0.20 M of BaNO$_3$ and 100 mL of reactive solution with 0.22 M of Na$_2$SO$_4$. Once the barite was precipitated, suspensions were centrifuged with Heraeus Megafuge 16R (Thermo-Scientific) for 5 min at 7000 rpm to separate the precipitates. The solids were then washed thrice with Milli-Q™ water to remove soluble salts, i.e., NaNO$_3$, and dried for BaSO$_4$ characterisation. In a second experiment, co-precipitation of Cs$^+$ and Sr^{2+} was carried out to study the removal efficiency of BaSO$_4$ for multiple ions. The addition of 25 ppm of each of Cs$^+$ and Sr^{2+} (from the nitrate salts) was made to the BaNO$_3$ solution prior to precipitation. Suspensions were again centrifuged, washed, and dried for analysis. The supernatants were filtered with a 0.3 μm syringe filter and analysed in a 240FS Atomic Absorption Spectrophotometer (AAS) (Varian-Agilent) to measure the final effluent concentration of Cs$^+$ and Sr^{2+} ions utilising a different wavelength and optimum working range for each metal ion (852.1 nm in 0.04–5 ppm concentration range for Cs$^+$ and 460.7 nm in 0.02–10 ppm concentration range for Sr^{2+}).

2.3. Pre-activation of natural clinoptilolite

Natural clinoptilolite was activated by sodium chloride salt (NaCl) with the aim of increasing removal capacity for the combined system. The pre-activation procedure was similar to those of Borai et al. [56] and Prajitno et al. [53]. Natural clinoptilolite was dispersed in a 1 M NaCl solution to give a 100 g/L solid/liquid ratio and mixed at room temperature for 24 h using a rotary carousel. The solution was then centrifuged, filtered, and rinsed with 300 mL of distilled water four times to reach the conductivity equilibrium, as indicated by Prajitno et al. [53], and washed with 25 mL of methanol for 1 h to dry.

2.4. Clinoptilolite adsorption kinetics

Clinoptilolite adsorption kinetics were analysed by mixing Cs$^+$ and Sr^{2+} solutions diluted to 25 ppm of each from 1 M stock solutions of SrNO$_3$ and CsNO$_3$ with Milli-Q™ water, to give a 20 mL total volume. In order to prevent Cs$^+$ adsorption onto glassware, polypropylene tubes were chosen to prepare aqueous solutions [57]. Natural or pre-activated clinoptilolite (0.4 g) was then added to give a fixed solid/liquid ratio of 20 g/L. All suspensions were then agitated with the IKA® HS 260 (IKA Works, Inc., Germany) orbital shaker at 150 rpm for different time periods (from 10 min to 24 h) at room temperature. Each suspension was centrifuged in a Heraeus Megafuge 16R (Thermo Scientific) for 10 min at 7000 rpm. Separated supernatants were filtered with a 0.3 μm syringe filter, whereupon Cs$^+$ and Sr^{2+} ion concentrations with AAS, using the same working ranges outlined in Section 2.2.

Measured ion concentrations were then used to calculate the Cs$^+$ and Sr^{2+} uptake by depletion in the given time as q_t (mg/g) and removal percent on both natural and activated clinoptilolite, using formulas defined as:

$$q_t = \frac{(C_o - C_e)}{m} \, V \tag{1}$$

$$\% = \frac{(C_o - C_e)}{C_o} \, 100\% \tag{2}$$

where C_o and C_e refer to initial and final concentration (ppm) respectively, with the mass of used adsorbent (m) and suspension volume (V).

Furthermore, the mechanism of adsorption kinetic in terms of adsorption rate was characterised using Pseudo-First Order (PFO) and Pseudo-Second Order (PSO) rate models, as shown in Eq. (3) and Eq. (4) respectively.

$$\frac{d_q}{d_t} = k_1 \, (q_e - q_t) \tag{3}$$

In Eq. (3) q_t and q_e (both mg/g) are the solute uptake at any time and at equilibrium, respectively, and k_1 (g/mg.min) is the rate constant of the PFO. For the PSO model (Eq. (4)) k_2 (g/mg.min) refers to the PSO rate constant, in which $1/k_2q_e^2$ and $1/q_e$ can be obtained from the gradient and intercept of $1/q$ vs. t respectively [53,58,59].

$$\frac{1}{q} = \frac{1}{k_2 q_e^2} + \frac{1}{q_e} \, t = \frac{1}{h} + \frac{1}{q_e} t \tag{4}$$

2.5. Combined clinoptilolite and BaSO$_4$ composite precipitation

Combined batch experiments were conducted by firstly mixing clinoptilolite prior to BaSO$_4$ precipitation, to give enhanced removal capacity and better particle sedimentation. As represented in Fig. 1, the first step was to disperse natural clinoptilolite into a conical flask containing 25 ppm of each Cs$^+$ and Sr^{2+} (at a 20 g/L solid/liquid ratio) in a total volume of 100 mL and mixed all at 300 rpm for 30 min to allow ion exchange to occur. The stirring speed was kept at 300 rpm to ensure a homogenous mixture and optimal decontamination factor, as evidenced in a previous study [55]. Then, 100 mL of 0.20 M Ba(NO$_3$)$_2$ was added and mixed for 5 min to prepare a reactive solution. Finally, 100 mL of 0.22 M NaSO$_4$ was fed into the solution and mixed for a further 10 min at 150 rpm to form the combined clinoptilolite-BaSO$_4$ precipitates. Then, the synthesised particle clusters were centrifuged and filtered for the determination of the removal efficiency of both radionuclides by AAS and were dried for particle characterisation. The same process was followed for an elevated natural clinoptilolite concentration (at 40 g/L solid/liquid ratio) and for NaCl-activated clinoptilolite.

2.6. Particle characterisation

Analysis was performed on the dried precipitated BaSO$_4$, the co-precipitated BaSO$_4$ with Cs$^+$ and Sr^{2+}, and composite material from the combined clinoptilolite system. The crystal structure was characterised by X-ray diffraction (XRD) using a D8 diffractometer (Bruker Corporation) at 40 kV and 40 mA, with a Cu Kα radiation source and step size of 0.024° for a 2θ scan range 15–70° for the BaSO$_4$ samples and 5–70° for clinoptilolite containing composite material. High-resolution scanning electron microscopy (SEM) (Hitachi SU8230) with Aztec Energy Dispersive X-ray (EDS) was used to analyse the morphology and elemental distribution of the particles. Samples were firstly coated with 10 nm thickness of carbon using Q150TE evaporative coater (Quorum) to make samples more conductive for SEM analysis. In addition, a High Angle Annular Dark Field (HAADF) Titan3 Themis 300 G2 (FEI, UK Ltd) Scanning Transmission Electron Microscopy (STEM) with a 100 pA beam current was operated at 300 kV to look at the deeper morphology of composite material and to show elemental distribution. Before STEM analysis, dried samples were dispersed well in methanol using an ultrasonic bath, and a drop from the dispersion was then put on a holey carbon-coated copper grid for analysis.

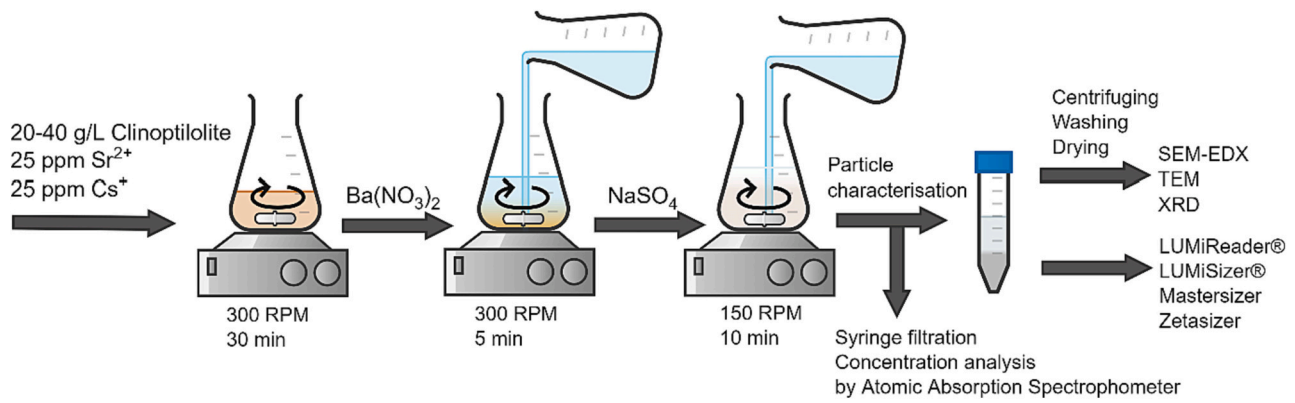Sedimentation and aggregate characterisation were performed to

Fig. 1. Schematic representation of the combined ion exchange and precipitation procedure.

determine the colloidal behaviour of particles for solid-liquid separation. Particle size distributions and gravitational sedimentation rates were studied using a Mastersizer 3000E laser diffractometer (Malvern Panalytical Ltd) and LUMiReader® X-Ray (L.U.M. GmbH), respectively. Additionally, zeta potential was measured as a function of pH using a ZetaProbe analyzer (Colloidal Dynamics Inc). Before the measurement, 10 mM of NaCl was mixed with solutions as a background electrolyte, while HCl and NaOH solutions were prepared at 0.25 M, and the pH was swept between 2 and 10 via an auto titrator.

Centrifugal sedimentation profiles for compressibility analysis were obtained from a LUMiSizer® 611 (L.U.M. GmbH) at 25 °C, applying an increasing centrifugal field from 500 to 3000 rpm. Compressive yield stress as a function of volume fraction was calculated from the centrifugal sedimentation profiles, according to the formulation established by Buscall and White [60], and Green et al. [61], as given in Eqs. (5) and (6). Compressive yield stress is an important parameter in wastewater sludges, to understand particle network behaviour under an external force, thus allowing the determination of liquid extractability from the suspension [62,63].

$$P_y\left(\varnothing_{eq}\right) = \Delta\rho g \varnothing_0 H_0 \left(1 - \frac{H_{eq}}{2L}\right) \tag{5}$$

$$\varnothing_{eq} = \frac{\varnothing_0 H_0 \left[1 - \frac{1}{2L}\left(H_{eq} + g\frac{dH_{eq}}{dg}\right)\right]}{\left[\left(H_{eq} + g\frac{dH_{eq}}{dg}\right)\left(1 - \frac{H_{eq}}{L}\right) + \frac{H_{eq}^2}{2L}\right]} \tag{6}$$

Here, $P_y(\varnothing_{eq})$ is the compression yield stress for equilibrium volume fraction ($\varnothing_{eq}$), and the density differences between solid and liquid are given as $\Delta\rho$, while g represents the centrifugal acceleration. The initial and equilibrium heights of the sediment are H_0 and H_{eq}, respectively, and the total distance from the sediment base to the centre of the centrifuge rotor is indicated as L. A schematic for the LUMiSizer® 611 cell showing the parameters for compressive yield stress is given in Electronic Supplementary Materials (ESM) Fig. S1. In the calculation of compressive yield stress, the applied centrifugal field plays an important role in the sedimentation bed, as more acceleration will result in a more compact bed due to particle aggregation [62]. Therefore, the applied force, namely relative centrifugal force (RFC) or g in the formula, must be determined for each increased rotation speed (RPM) using the conversion Eq. (7):

$$RCF = 1.118 \times 10^{-5} \times r \times RPM^2 \tag{7}$$

where r is the radius distance to the sediment bed bottom in centimetres. RPM was converted into RCF by taking the rotor distance (r) as 13 cm for each acceleration from 500 rpm to 3000 rpm as given in Table 1. Once RFC was determined, the derivative between the equilibrium sediment

Table 1
Conversion of rotor speed to the relative centrifugal force (RFC) in the LUMiSizer®.

RPM	RCF (x g)
500	36.34
1000	145.34
1500	327.02
2000	581.36
2500	908.38
3000	1308.06

height (H_{eq}) and the relative centrifugal force (RCF), dH_{eq}/dg in the formula, was calculated by fitting the data to a power-law model, using Microsoft Excel™ (where the derivative function was, thus, easy to determine). This procedure enabled the calculation of $\varnothing_{eq}$ for all the measured RPMs.

3. Results and discussion

3.1. Mineralogy and morphology of synthesised particles

High-resolution SEM images of single clinoptilolite and precipitated BaSO$_4$, along with the combined composite system, are shown in Fig. 2 for a morphological comparison. From Fig. 2a, clinoptilolite particles have a roughened crystalline surface where fine grains are attached, arising from high particle friability, which allows for easy mechanical milling to increase the specific surface area for enhanced adsorption performance [53,64,65]. BaSO$_4$ particles appear as irregular, spheroidal nanosized objects that are clustered together (Fig. 2b). As stated by Ramaswamy et al. [66], the spherical morphology of BaSO$_4$ particles may indicate that the particles possess minimum water content. Bolaina-Lorenzo et al. [67] also characterised precipitated BaSO$_4$ particles as prolate-spherical agglomerates, while this finding additionally reflects those of Flouret et al. [45] who also found that BaSO$_4$ was defined as loose agglomerates of nanocrystals.

As for the combined system, the SEM image in Fig. 2c reveals that the larger, fractured clinoptilolite material appears to be partially covered by BaSO$_4$ crystals and coagulated together. Furthermore, an elemental mapping of the combined system from energy-dispersive X-ray spectroscopy (EDS) is given in Fig. 2d, where it is clear that mixed clusters of BaSO$_4$ and clinoptilolite reside together while being distributed across the sample surface. The coagulation mechanism of composites is perhaps based on the bridging effect initiated by Ba^{2+} ions adsorption on the clinoptilolite surface for BaSO$_4$ formation, which creates a loose core-shell structure with the zeolite surrounded by the precipitated BaSO$_4$ [68,69]. In addition, peaks from the EDS are given in the ESM (Fig. S2) for precipitated BaSO$_4$ and the combined system, which again inferred the two species were fairly homogenously coagulated across the
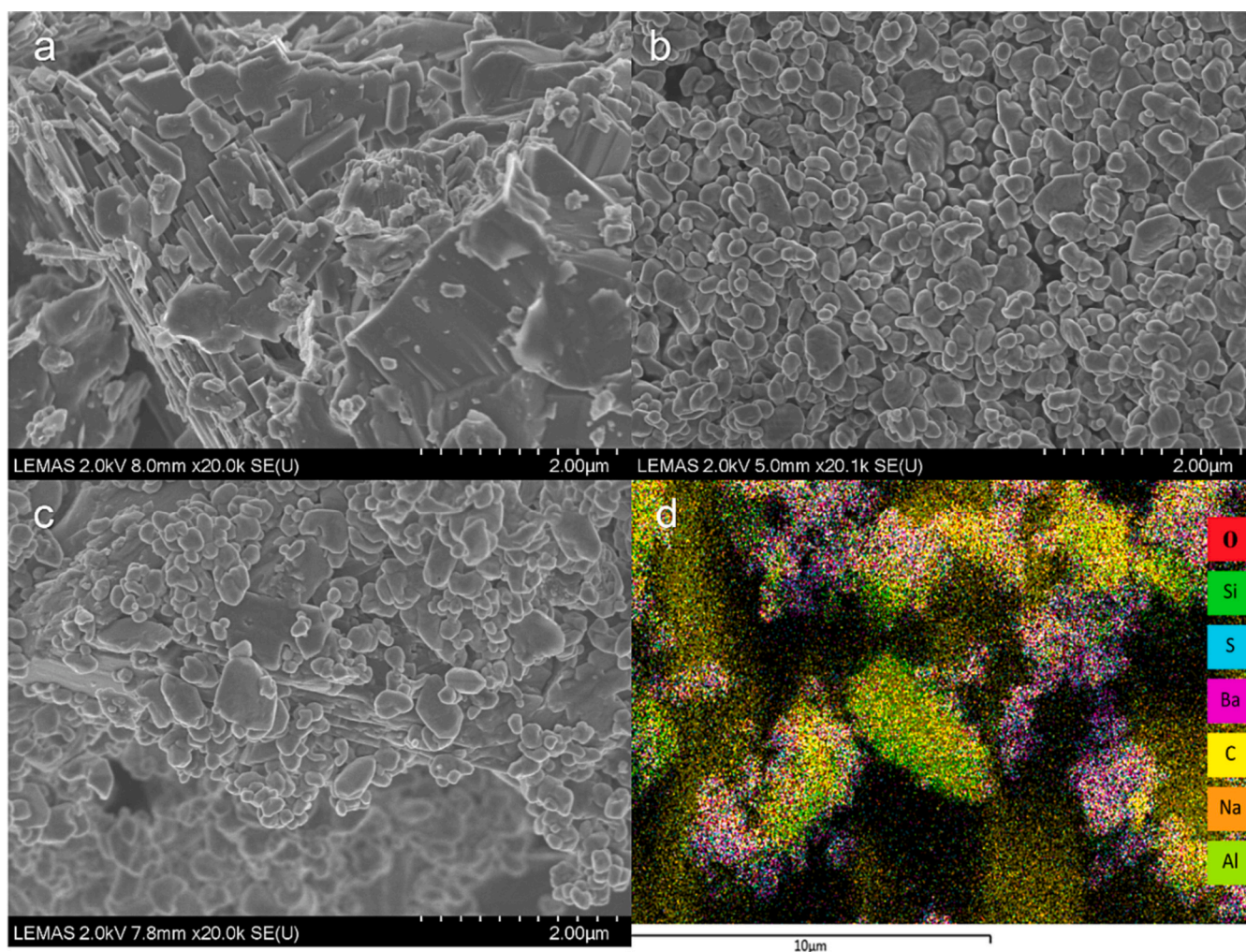
Fig. 2. High-resolution scanning electron microscopy (SEM) of a) natural clinoptilolite, b) precipitated BaSO$_4$, c) combined composite of clinoptilolite and BaSO$_4$ particles with Cs$^+$ and Sr^{2+}, and d) energy-dispersive x-ray spectroscopy (EDS) image of the composite coagulant.

sample. Noteworthy, no peaks were detected in the EDS analysis for Cs$^+$ and Sr^{2+} due to the limit of detection. Trace species such as potassium and iron were detected, which are likely existing contaminants present in the clinoptilolite.

High Angle Annular Dark Field (HAADF) scanning transmission electron microscopy (STEM) was used to analyse the composite material and show the local elemental distribution of the BaSO$_4$ and clinoptilolite to a high special resolution of a single grain, as given in Fig. 3. It is observed that BaSO$_4$ is mostly located on the clinoptilolite surface while precipitating together giving brighter region on HAADF image (see also the relative concentrations of Ba and S on the upper section). On the lower section, there is a region of relatively bare clinoptilolite (with low Ba and high Si levels). This region also shows areas occupied by iron and potassium, which are known as the two main contaminants of clinoptilolite, which affect Cs$^+$ and Sr^{2+} uptake adversely due to mineral impurities and ion competition [27,53]. Potassium, in particular, is responsible for low Cs$^+$ uptake, as they have close hydrated ionic radii and hydration enthalpies to each other [70,71]. Despite causing lower Cs$^+$ uptake, the competition between K$^+$ and Cs$^+$ has been used to prevent Cs$^+$ bioaccumulation by plants by applying potassium fertilisers for Cs$^+$ contaminated areas [72].

As for the mineralogy of synthesised crystals, X-ray diffraction patterns were obtained to characterise the crystal structures of BaSO$_4$ particles and the combined system. In Fig. 4, the main diffraction peaks of precipitated BaSO$_4$ are given and are in good agreement with the

reference peaks. Also shown is coprecipitated BaSO$_4$ with the direct addition of 25 ppm Cs$^+$ and Sr^{2+} (i.e., without the addition of ion exchange) which presents a consistent diffraction pattern to the pure BaSO$_4$, inferring no crystallographic changes occur with these low levels of heavy metals. The hkl values of diffracted peaks were defined with a JCPDS card (no: 00–005-0448) for BaSO$_4$, confirming that the particles are BaSO$_4$ and indexed to an orthorhombic crystal system and Pbnm space group. The pure BaSO$_4$ has slightly sharper (narrower) peaks, indicating perhaps some enhanced crystallinity compared to the precipitated BaSO$_4$ with Sr^{2+} and Cs$^+$, which have greater peak broadening. A possible explanation for this might be that Sr^{2+} and Cs$^+$ ions may lead to Scherer broadening that decreases the crystallinity, as evidenced in a previous study by Akyol et al. [73]. Also, there is a little offset in peaks observed for the BaSO$_4$ data with respect to the combined system, which may be due to the difference in crystal size and the composition in the combined system that may influence the BaSO$_4$ peak shift. XRD patterns of the combined system are also given in Fig. 4 with clinoptilolite reference peaks (no: 04-013-6125) where it is seen that the diffracted peaks for the combined system mostly comply with the BaSO$_4$ crystal structure. Peaks for clinoptilolite appear only in the first 2θ area and suffer from peak intensity reduction likely due to being the supporting material in the combined system [58]. XRD peaks for natural clinoptilolite along with the reference peaks are presented in the ESM (Fig. S3) presenting a good fit to a Ca-type clinoptilolite zeolite structure [74].
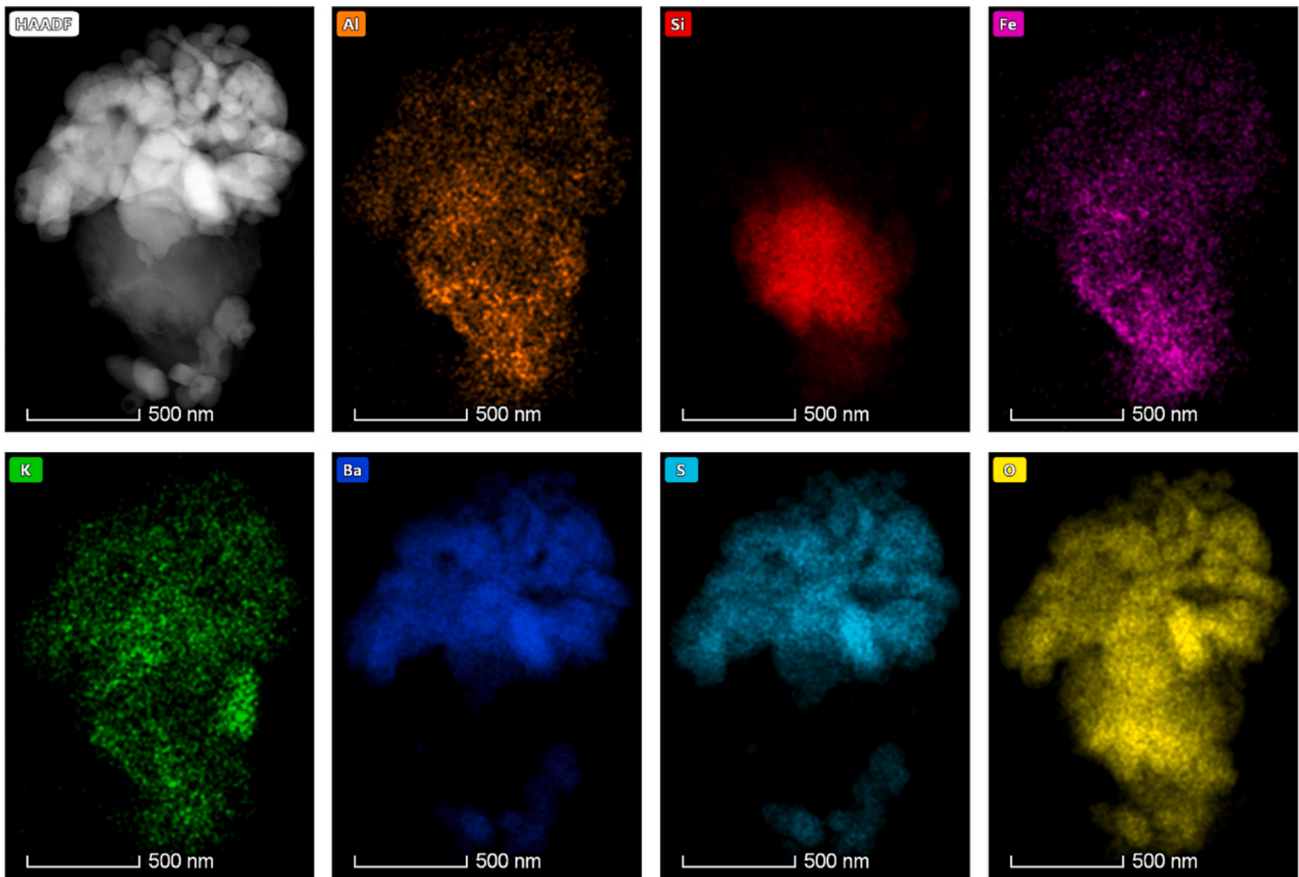
Fig. 3. Transmission electron microscopy (TEM) of coagulated composite particles in the combined system, containing clinoptilolite and $BaSO_4$ precipitated with 25 ppm of each Cs^+ and Sr^{2+}.
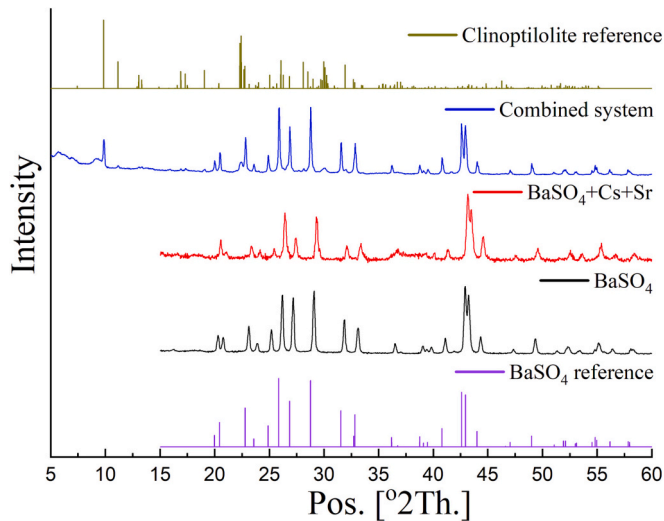

Fig. 4. X-ray Diffraction (XRD) patterns of pure precipitated $BaSO_4$ (black), co-precipitated with 25 ppm of each Cs^+ and Sr^{2+} (red) and coagulated composite particles in a combined system with clinoptilolite (blue). Also given are reference peaks for $BaSO_4$ (purple, no: 00-005-0448), and clinoptilolite (green, no: 04-013-6125).

Fig. 5. Particle size distributions of precipitated $BaSO_4$, natural clinoptilolite, and the combined composite (containing co-precipitated $BaSO_4$ and natural clinoptilolite).

3.2. Aggregation and sedimentation

Particle size distributions are given in Fig. 5 for the synthesised $BaSO_4$, the combined system (ion exchange and precipitated $BaSO_4$),
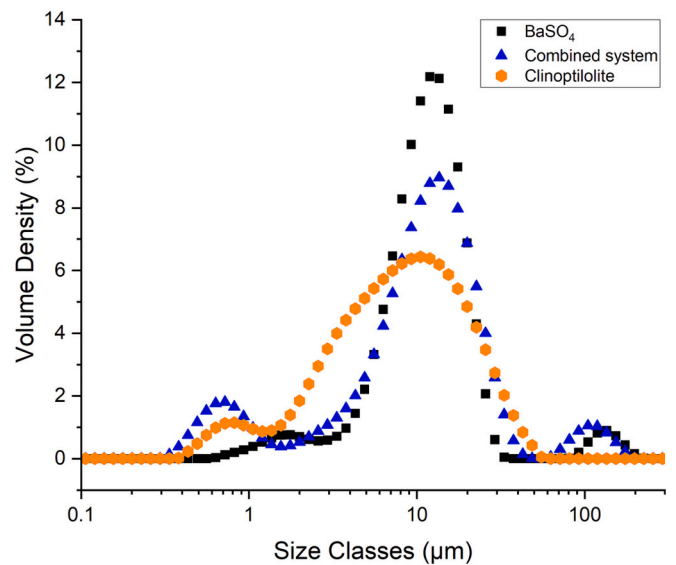
and natural clinoptilolite. The $BaSO_4$ and combined system follow multimodal distributions, with, however, clear primary peaks of similar mean sizes at ~12 μm, and are dominated by the agglomeration of $BaSO_4$ crystals in a supersaturated solution [75]. Moreover, the ionic strength plays an important role in the agglomeration process in which it

enlarges the particle sizes, due to the relatively high sodium nitrate and sulphate levels reducing double-layer repulsion [45]. Both the $BaSO_4$ and combined systems also display a small further aggregate peak at +100 μm, which is likely a small proportion of higher-order aggregate clusters. The low proportion of larger clusters may be due to the relatively high shear rate within the Mastersizer cell, which is known to break down weaker aggregates [76].

As for clinoptilolite, it has a peak size broadly within manufacturer estimates at ~10 μm and is in line with similar fine-milled material [77,78]. There is also a small clear fine peak below 1 μm, which is likely due to particulate breakage because of the friable nature of the material [79]. The combined system appears to largely aggregate the smaller micron-sized fines into the composite clusters, although, the presence of some submicron fines remains in the distribution.

The zeta potential as a function of pH with background electrolyte was performed for all systems, and averaged data taken from each analysis is presented in Fig. 6. $BaSO_4$ presents a positive zeta potential across a wide pH range, although its magnitude decreases at higher pH due to the attraction of OH^- ions onto the $BaSO_4$ surface. The isoelectric point (IEP) for $BaSO_4$ was not determined, with some evidence of a variable IEP in $BaSO_4$ being reported in the literature [80,81]. The variation of zeta potential values for $BaSO_4$ has been explained by Bracco et al. [82], who stated that the surface charge is not a fundamental property of $BaSO_4$ and is significantly affected by surface defects or charge imbalances caused by impurities. It is noted also that the low magnitude of the zeta potential measured (~5 mV at neutral pH) indicates a low level of electrostatic repulsion, which leads to cluster aggregation.

By contrast, clinoptilolite was observed to remain strongly negatively charged throughout the pH range tested. It was not possible to measure lower pH levels towards the IEP, due to the ion exchange of H^+ ions with the clinoptilolite surface [83], causing a continual shift to higher pH levels [53]. Given the opposite charges between the $BaSO_4$ and clinoptilolite, it further suggests the strong interaction between the precipitating species, and indeed, the zeta potential behaviour for the combined system is a combination of the two particulates. Here, the surface charge of the precipitated clusters was positive until neutral pH where IEP was determined. As seen, the surface charge reached negative values after pH 7 due to the addition of OH^- ions and then started being more negative. It is interesting that the overall zeta potential is more similar to the $BaSO_4$ than the clinoptilolite. This trend can be supported by the explanation that the $BaSO_4$ appears to dominate the measured zeta potential charge, as it is largely precipitated on the outside of clinoptilolite grains [82]. Overall, according to the stability criteria, zeta
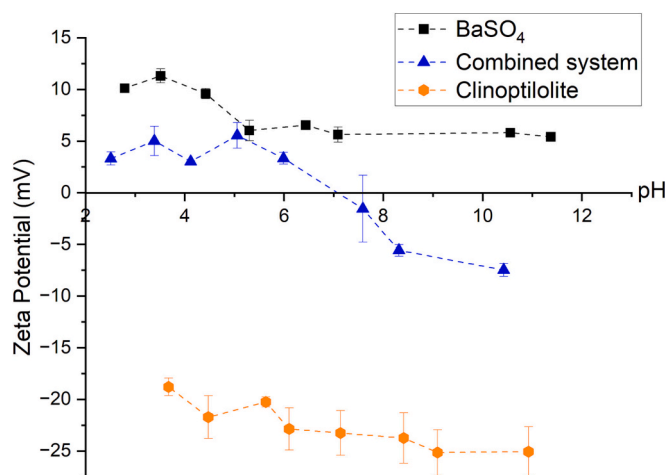
potential data highlights that suspensions are considered unstable, as they are all distributed between −30 and +30 mV [84].

The sedimentation analyses under the Earth's gravitational force, and under the different centrifugal forces, were studied to examine the aggregates settling and consolidation behaviour. Real-time vertical settling profiles under Earth gravity with linear region settling rates (shown as dashed lines) are given in Fig. 7, as measured by the x-ray profiler. The final bed fractions for the solid concentration under the interface region were also calculated and presented as an inset figure in Fig. 7, by taking the initial and final bed heights of each suspension with their volume fraction. Presented is data on $BaSO_4$ flocs with and without co-precipitation of Cs^+ and Sr^{2+}, along with the combined system with ion exchange. Raw transmission data and repeat profiles are shown within the ESM (Fig. S4).

It can be observed that all three systems show similar settling trends, which may be expected from the similar aggregate sizes, with sedimentation occurring within the first 50 s, before entering the compressional zone [85,86]. Nonetheless, the initial setting rate of the combined system was almost twice as fast (see Fig. 7 inset), highlighting that the density of the composite flocs is likely greater than the pure $BaSO_4$ agglomerates, and indicating one critical advantage of the composite system. There was also no significant difference of $BaSO_4$ flocs with or without heavy metal coprecipitation, inferring no difference in floc size, consistent with the lack of crystalographic changes (Fig. 5). It is also noted that the settling profile of pure clinoptilolite was tested (see ESM, Fig. S5) with the fine non-aggregated nature of the particles producing a slow diffuse settling behaviour, highlighting that agglomeration with barite is required to accelerate the sedimentation. Overall, given the similar floc sizes, it is assumed that the cause of the enhanced sedimentation rates is primarily from the composite core-shell aggregates being much denser than $BaSO_4$ precipitates with a lower water content [68,69]. Such distinction infers a very strong association between the species with the combined precipitation method and good stability for forward processing.

Indeed, regarding the final settled bed volume fractions (Fig. 7(b) inset), it can be observed that the combined system not only settled faster but consolidated much more significantly compared to $BaSO_4$ in the absence of any additional compressive force, which highlights a desirable dewatering capacity. The final volume fraction of the combined system was elevated to some degree from the greater initial
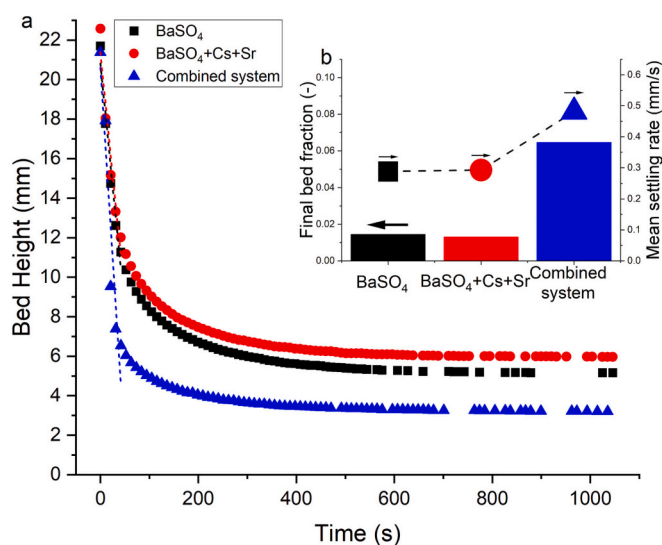
Fig. 6. Zeta potentials for all studied systems with background electrolyte (10^{-2} M NaCl). Error bars represent the standard deviation from the mean values.

Fig. 7. (a), X-ray sedimentation rates for pure $BaSO_4$ (black) and with Cs^+ and Sr^{2+} ions (red) and the combined system (blue) containing clinoptilolite and $BaSO_4$ with both ions. Dashed lines represent linear fits to the settling region. Inset (b), the final bed volume fractions (left-hand axis) and mean settling rate (right-hand axis).

volume fraction, due to the added clinoptilolite. However, the compression ratio between the initial and final volume fractions is still much larger than the BaSO$_4$-only systems (nothing the final bed height is lower for the combined system, despite the initial volume fraction being larger from the clinoptilolite inclusion). This difference suggests that as well as aiding the removal of Cs$^+$ from ion exchange, the zeolite is acting as a weightier material, allowing higher levels of dewatering and lower final waste volumes from the denser flocs, of critical importance in the nuclear industry.

Sedimentation profiles and yield stress analysis were studied for various centrifugal accelerations in the LUMiSizer® to understand the particle network behaviour under applied stress. Fig. 8 presents the sedimentation profiles for pure BaSO$_4$, BaSO$_4$ with co-precipitated Cs$^+$ and Sr^{2+}, and the combined system with ion exchange, under variable centrifugal acceleration from 500 rpm to 3000 rpm (illustrated by dashed lines). Example transmission profiles and repeated analysis are given within the ESM (Fig. S6). It can be observed that all suspensions formed their initial bed height of approximately 2.5 mm in the first minute at 500 rpm with stepwise changes in bed heights, i.e. higher compression, being obtained with increased centrifugal fields up to 3000 rpm, which gave an average of 1.16 mm of their compressed final bed heights. Under compression, the differences in sediment height between the combined system with the BsSO$_4$ flocs were less than under Earth gravity, although, given the higher initial volume fractions of the combined system, the level of dewatering attainable was still impressive. As described in the literature [62], stable particles cannot be further compressed due to forming close particle arrangements, while aggregated particles undergo additional compression with increased centrifugal force due to a loose particle network. Therefore, additional compression to the sedimentation beds observed for each suspension are likely due to the particle aggregation, supported by the Mastersizer analysis given in Fig. 5.

Compressive yield stress, i.e. $P_y(\phi)$, is another key measurement for colloidal systems to determine the network strength of the particles in a formed sedimentation bed under compression at applied centrifugal force [60]. Based on this approach, it can be understood to what extent suspensions can be physically separated, or dewatered, as the liquid is extracted to produce a closer network from the applied force [60,62]. The level of dewatering is dependent on this compression yield stress
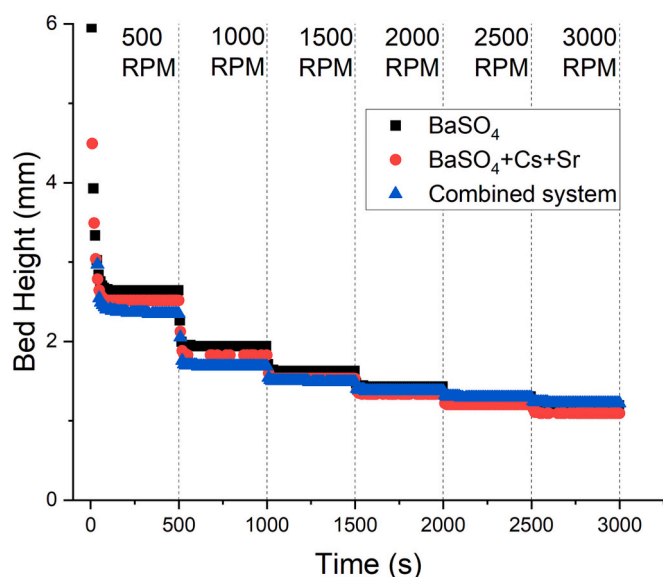
that must be overcome for consolidation [63,87]. In Fig. 9, the calculated compressive yield stress, $P_y(\phi)$, based on the centrifugal sedimentation profiles, is given with an exponentially fitted curve.

It is evident that the BaSO$_4$ and BaSO$_4$ + Cs + Sr flocs exhibited low initial bed density with 0.026 and 0.028 v/v at the same pressure of 0.339 kPa, respectively. As a result of weaker network strength and aggregate formation, equilibrium BaSO$_4$ volume fraction were more than doubled at higher yield stresses, indicating that BaSO$_4$ suspensions are a highly compressible material at low to moderate pressures [87]. For the combined system, while the yield stress range was larger, compression critically occurred over much greater volume fractions. The gel point was observed at an initial pressure of 0.955 kPa due to the addition of clinoptilolite, rising to a pressure of 8.6 kPa under 3000 rpm. However, the corresponding equilibrium volume fractions increased from 0.077 to 0.153 v/v, approximately three times higher than the BaSO$_4$-only systems. The BaSO$_4$ suspensions did experience a slightly greater compression ratio as centrifugal acceleration was increased, compared to the combined system, which may be due to the increased floc density of the aggregates in the combined system [60,63]. Overall, the characterisation of aggregates proves that combined BaSO$_4$ and clinoptilolite composite flocs are observed to give rapid sedimentation and higher levels of compression, of great importance for solid-liquid separation.

3.3. Removal efficiency of combined batch experiments

An initial adsorption kinetics study was carried out using 20 g/L of natural clinoptilolite for a mixed metals solution containing 25 ppm of each Cs$^+$ and Sr^{2+} ion with different agitation times. In Fig. 10(a), the adsorbed amount of natural clinoptilolite for Cs$^+$ and Sr^{2+} is given as q_t (mg/g) and removal percentage, where the adsorption equilibrium is reached after ~1 h, giving 96.7 % and 89.7 % removal efficiency of Cs$^+$ and Sr^{2+} ions, respectively. As expected, lower Sr^{2+} uptake was observed in natural clinoptilolite as a result of lower affinity, consistent with previous works [27,53]. Also as stated, the higher Cs$^+$ selectivity of clinoptilolite might be due to its narrow channels with small pore sizes between 3.5 and 3.9 Å that is suitable for hydrated Cs$^+$ ions (3.45 Å) and favourable high Si: Al ratio of clinoptilolite [30].

Based on Eqs. (3) and (4), Pseudo-First Order (PFO) and Pseudo-Second Order (PSO) rate models were studied to determine the rate constants according to the adsorption kinetics. The adsorption kinetics
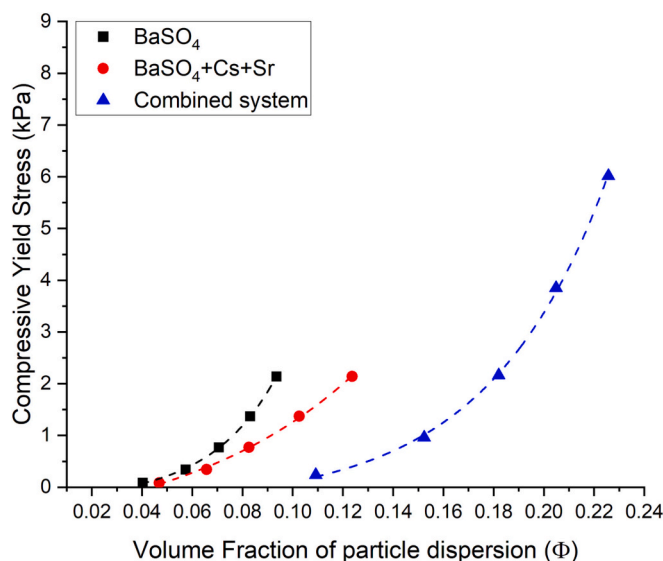

Fig. 8. The sedimentation of BaSO$_4$ (black), BaSO$_4$ with Cs$^+$ and Sr^{2+} ions (red), and combined system synthesised with clinoptilolite and BaSO$_4$ under centrifugation at various speeds (500–3000 rpm). Vertical dotted lines indicate the acceleration in centrifugation.

Fig. 9. Compressive yield stress of BaSO$_4$ (black), BaSO$_4$ with Cs$^+$ and Sr^{2+}(red), and combined composite with clinoptilolite and BaSO$_4$ with ions (blue) from LUMiSizer® analysis. Dashed lines indicate power-law fits.
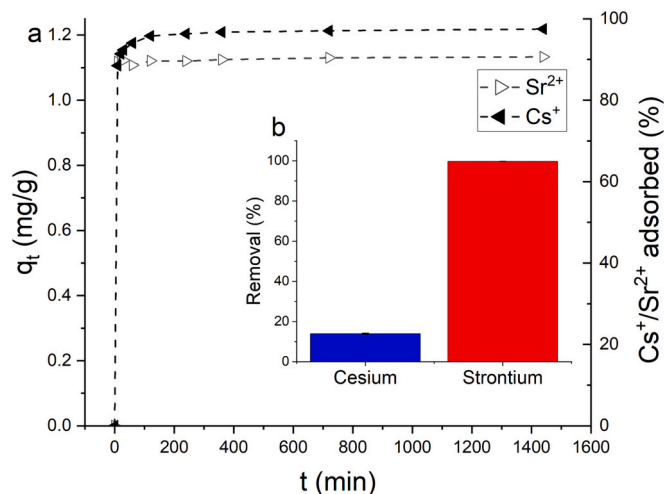
Fig. 10. Adsorption kinetics of natural clinoptilolite for 25 ppm of Cs^+ and Sr^{2+} ions with different adsorption times, from 15 min to 24 h (a); the left vertical axis represents adsorption per mass of ion exchange and right vertical represents removal percentage. Removal efficiency from $BaSO_4$ precipitation for Cs^+ and Sr^{2+} (b) Inset.

are in good agreement with the PSO model being used to fit the kinetics as shown in Fig. 10(a). The difference in the regression coefficient for PFO and PSO rate models can be found in ESM (Fig. S7). The PFO plots in Fig. S7 are observed to have a slightly smaller R^2 (< 0.9) and thus would suggest kinetics follow a PSO model more closely. Application of the PSO model confirms that the rate-limiting step is predicted as chemical interactions via surface energy changes (i.e. chemisorption) which is common for specific ion exchange sites on zeolites and other related materials [53,58,88–90]. Apart from the chemisorption, physical adsorption, i.e., physisorption, may also play a role in the electrostatic interactions of cations (Cs^+ and Sr^{2+}) with the negatively charged clinoptilolite surface. It is noted that it is not normally possible to distinguish surface adsorption via electrostatics or ion exchange on clinoptilolite, owing to their fairly similar adsorption energies and that accessible ion exchange interactions are also from surface or near-surface sites [53].

The calculated rate parameters for both PFO and PSO models are presented in Table 2. Accordingly, the PSO model followed the general trend producing a higher initial adsorption rate (h) than the overall PSO rate constant (k_2) [27]. The PSO rate constant (k_2) for Cs^+ was faster than found for larger granular clinoptilolite previously [53], but similar to previous rates found for fine milled clinoptilolite [78]. Interestingly, the PSO rate constants for Sr^{2+} were comparably higher than Cs^+, although the PFO model rate constants were lower. This discrepancy is likely due to the fact that adsorption was relatively rapid in both cases, where ion transportation to larger pores governs the adsorption kinetics for both ions, even if the equilibrium amount of Cs^+ sorbed was clearly

Table 2
Pseudo-second order rate constants (k_2), initial adsorption rates (h), and adsorbed solute amount at equilibrium (q_e) from dynamic uptake tests of 25 ppm solutions of Cs^+ and Sr^{2+} with natural clinoptilolite. Pseudo-first order rate constants (k_1) are also given for comparison.

PSO				PFO
Cs^+				Cs^+
k_2	h	$q_{e,cal}$	$q_{e,exp}$	k_1
(g/mg.min)	(mg/g.min)	(mg/g)	(mg/g)	(min^{-1})
0.384	0.571	1.219	1.218	0.004
Sr^{2+}				Sr^{2+}
k_2	h	$q_{e,cal}$	$q_{e,exp}$	k_1
(g/mg.min)	(mg/g.min)	(mg/g)	(mg/g)	(min^{-1})
0.711	0.913	1.133	1.132	0.002

higher than Sr^{2+} [91,92]. Additionally, also consisted with the literature, the PFO rate model had larger fitting errors in both cases [93].

$BaSO_4$ co-precipitation of 25 ppm of Sr^{2+} and Cs^+ was also studied to understand the simultaneous removal efficiency of $BaSO_4$ precipitation in the scope of nuclear effluent treatment. As observed in Fig. 10(b), the removal efficiency of Sr^{2+} with $BaSO_4$ is seven-fold higher than Cs^+, which is because of similar ionic radii and valency of Sr^{2+} to that of Ba^{2+} (Sr^{2+} 1.21 Å, Ba^{2+} 1.44 Å, Cs^+ 1.88 Å) [94]. Hence, Sr^{2+} selectively interacts with barite crystals through incorporation into the $BaSO_4$ crystal structure, or alternatively, via adsorption onto the $BaSO_4$ surfaces by forming inner/outer-sphere complexes [82,94]. The higher affinity of Sr^{2+} to $BaSO_4$ is supported by Tokunaga et al. [94] who calculated the distribution coefficients (K_d) of multiple ions including Sr^{2+} (5.8×10^6 L/kg) and Cs^+ (2.6×10^0 L/kg), indicating the importance of close ionic radii of Sr^{2+} to Ba^{2+} ions. As evidenced here, the simultaneous removal of both ions using only $BaSO_4$ precipitation is not achieved, and hence improvements or alterations are required to increase Cs^+ removal efficiency.

Following the understanding of the sorption mechanism of clinoptilolite, combined batch adsorption was conducted, initially with clinoptilolite for 30 min, followed by $BaSO_4$ precipitation (as represented in Fig. 1). Initially, 20 g/L of natural clinoptilolite was dispersed to the Cs^+ and Sr^{2+} containing solution prior to $BaSO_4$ precipitation and the removal efficiency of the combined system is presented in Fig. 11 (orange bars).

It is apparent from the results that Sr^{2+} was captured more efficiently, achieving 99.9 % removal, while Cs^+ showed lower performance in the combined system giving 82.8 % removal. These findings suggest that clinoptilolite adsorption dominates Cs^+ removal efficiency in the combined system, owing to low Cs^+ interaction with $BaSO_4$. However, unfortunately, Cs^+ removal was actually lower in the combined system than for clinoptilolite only (which removed ~91 % after 30 min). It is assumed this is because Ba^{2+} ions may interfere with Cs^+ adsorption and reduce efficiency after the $Ba(NO_3)_2$ is added, as Ba^{2+} is known to be exchanged by clinoptilolite in literature [95]. It should be noted that the cation selectivity of clinoptilolite for these three cations is provided as $Cs^+ > Ba^{2+} > Sr^{2+}$, which proves that Ba^{2+} may lead to a matrix effect [96,97]. Additionally, the type of clinoptilolite can affect its ion exchange performance as its mineralogy varies depending on the geology of where it is mined [98]. As a result, it was decided to increase the clinoptilolite solid-liquid ratio to 40 g/L (Fig. 11, purple bars). The effect of increased clinoptilolite improved Cs^+ removal marginally, while a minor effect was observed for Sr^{2+} remaining almost the same at 99.9 % due to having a higher percentage in all systems.
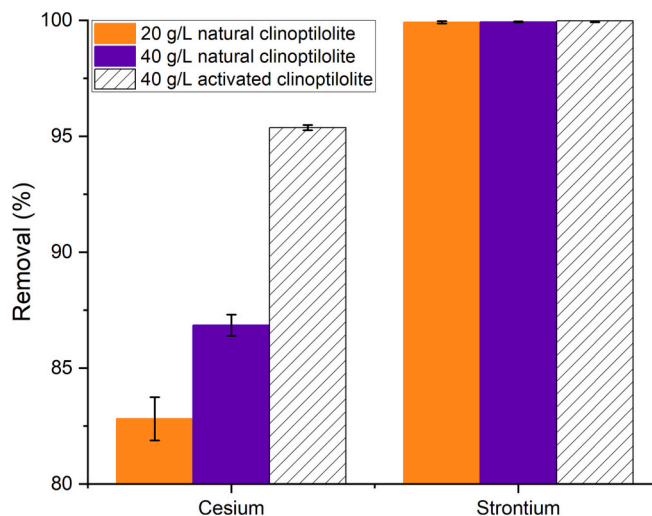

Fig. 11. Total removal percent of Cs and Sr in a combined system with different clinoptilolite conditions; 20 g/L, 40 g/L natural, 40 g/L NaCl treated.

To further improve the clinoptilolite, and more fully compensate for the exchange of Ba^{2+}, pre-activation of the zeolite by NaCl was also undertaken. As evident in the literature [99–101], NaCl treatment can enhance the removal efficiency leading to the homoionic form, namely Na-form, of clinoptilolite, where Na^+ ions can easily be exchanged with target cations owing to weaker Na bonds to the clinoptilolite structure. There was a decision to focus on pre-activation with NaCl rather than acid, for example, as previous work has shown adsorption capacity with NaCl treatment for both Cs^+ and Sr^{2+} ions in all concentration ranges [53]. Additionally, HCl treatment might cause the destruction of adsorption sites which decreases the exchange capacity, even if it is assumed to clean the pores and increase surface area [53,78,99,101]. The effect of NaCl activation compared to natural clinoptilolite in kinetic studies of zeolite suspensions is provided in Fig. S8 of the ESM, where the increase in adsorption is evident for both Cs^+ and Sr^{2+}. Noteworthy, it suggests that pre-treatment might also be responsible for reducing interference effects, such as K^+, especially for Cs^+, which was shown to cover a relatively large area in the TEM results (Fig. 3) [53].

The results for the combined coagulated system with activated clinoptilolite are also given in Fig. 11 (shaded bars), confirming that NaCl-treated clinoptilolite significantly enhanced the Cs^+ adsorption (>95 %), as well as effectively complete Sr^{2+} removal (> 99.9 %). To highlight the overall performance of the combined composites, the simultaneous removal efficiencies of Cs^+ and Sr^{2+} are compared to other recent studies using a variety of materials in Table 3. It is noted, importantly, that investigations considering suitable materials for simultaneous high-level adsorption for Cs^+ and Sr^{2+} are limited due primarily to the difference in their valence state and ion size, as discussed. In all cases, a compromise is required between cesium and strontium removal performance, with most studies showing greater cesium removal. In comparison, the current core-shell composites achieve superior efficiency for Sr^{2+} ions while achieving desirable Cs^+ removal in a single system.

There is still some evidence of a very small percentage of Cs^+ being remobilised with the activated clinoptilolite from the exchange with Ba^{2+} (if one compares Cs^+ removal to the pure ion exchange). Still, the advantages of the combined system, in terms of enhanced dewatering, make such composite flocs a practical route to both give high adsorption and more efficient forward processing. The fact that the combined flocs both settle faster and consolidate to a significantly greater degree means they could be separated either gravitationally or centrifugally producing considerably reduced intermediate-level waste volumes. Additionally, the presented two-step method for producing the composite flocs is operationally simple (requiring only a single continuously stirred tank reactor, CSTR). Thus, the clinoptilolite could be incorporated for additional benefits in many existing precipitation operations without the need for extensive plant retrofitting.

It is pertinent to further consider the downstream industrial implications for the use of such combined coagulated materials. As reported,

ion exchange and $BaSO_4$ are separately proven techniques to remove radioactive Cs^+ and Sr^{2+}, for example at Fukushima, although there they are used in separate operations and produce and high secondary waste volumes [42]. However, combining clinoptilolite and $BaSO_4$ can overcome the efficiency and waste issues encountered and offer an industrially viable and economical solution, due to the use of a single operational unit. Additionally, the use of a single mixing unit would allow for its process intensification, using intensified plug-flow reactors to overcome innate mixing inefficiencies of CSTRs. For example, previous work by Tonge et al. [49], considered the use of an agitated tubular reactor to intensify the production of composite coagulants for dye removal, and it is thought that similar designs could be adapted for use in nuclear effluent clean-up [35].

Moreover, regarding post-treatment management, the remaining radioactive waste will be immobilised using an appropriate solidification/encapsulation matrix, before the solid encapsulate is prepared for long-term storage and disposal [106]. Therefore, the enhanced separation and dewatering characteristics would not only reduce waste volumes requiring solidification but should allow higher density encapsulates with lower additives. It is noted that the regeneration of the ion exchange or coagulants would not generally be industrially considered, as this would lead to a re-release of radiation, and the precipitates are not re-used anywhere currently in nuclear waste treatments. Cementation with ordinary Portland cement (OPC) is a widely adopted and used method for the encapsulation of low-level (LLW) and intermediate-level (ILW) wastes in the UK, with the combined coagulant wastes likely categorised as ILW [107,108]. In addition to cement-based technologies, alternatives such as geopolymers or glass composites are also studied and used to encapsulate Cs^+ and Sr^{2+} doped adsorbents [108–110]. As for $BaSO_4$ precipitates, it is evidenced that cementation has been shown to encapsulate $BaSO_4$-containing wastes after ^{226}Ra removal [111]. Hence, the composite flocs containing clinoptilolite and $BaSO_4$ might be encapsulated through an OPC system and can be stored safely as sludge cake, although further studies should assess the performance of OPC for composite flocs encapsulation.

4. Conclusions

The present research investigated the simultaneous removal of cesium and strontium ions by combining fine clinoptilolite and precipitated barite ($BaSO_4$) to allow the development of composite core-shell coagulants with enhanced sedimentation for solid-liquid separation. In batch conditions, $BaSO_4$ crystals and composite coagulants were successfully precipitated, and their mineralogy and morphology were subsequently characterised by SEM, STEM, and XRD. Results indicated that the composite coagulants were in a loose core-shell structure, where the clinoptilolite was decorated by precipitated $BaSO_4$ particles with the distinct crystallographic zeolite and barite phases being present and unaltered. Aggregate size, sedimentation behaviour and the compressional yield stress were also analysed to determine separation efficiency and suspension dewaterability. The combined coagulates were shown to settle almost twice as fast as $BaSO_4$ alone, and produced more consolidated beds, suggesting the clinoptilolite acted as weighter material to densify formed aggregates. Centrifugal yield stress tests also indicated that the combined coagulants produced high volume fraction beds with enhanced mechanical dewaterability. As a result, the composite coagulation formed by the addition of clinoptilolite contributes to particle sedimentation and compression, which reduces the overall volume of sludge to be treated downstream.

Regarding metal ion removal efficiency, $BaSO_4$ removed a very high amount of Sr^2, whereas it was not effective in extracting Cs^+ ions owing to inappropriate ionic radii to the $BaSO_4$ crystal structure. To compensate for low-level Cs^+ removal efficiency, clinoptilolite was utilised as an ion exchanger to adsorb Cs^+ ions and a portion of the Sr^{2+} before $BaSO_4$ precipitation. Additionally, an adsorption kinetic study of natural clinoptilolite was performed for 25 ppm of both Cs^+ and Sr^{2+} ions

Table 3
Comparison of combined composite clinoptilolite-$BaSO_4$ for simultaneous removal of Cs^+ and Sr^{2+} in comparison to existing literature.

Material	Concentration (ppm)		Maximum efficiency (%)		References
	Cs^+	Sr^{2+}	Cs^+	Sr^{2+}	
$BaSO_4$ + clinoptilolite (current study)	50	50	95.3	99.98	This study
Thermally treated natural zeolite	50	50	99.3	94.5	[93]
Prussian blue immobilised alginate aerogel	100	100	~97	~80	[102]
Modified hydroxyapatite	100	100	99	85	[103]
Stannic molybdophosphate in polyacrylamide	–	–	>90	>90	[104]
Free-standing titanate nanobelt (TNB) membranes	–	–	62.5	98.5	[105]

simultaneously, where they obeyed a Pseudo-Second Order model in good agreement with literature. Composite coagulants were then produced using 20 g/L and 40 g/L of natural clinoptilolite and BaSO$_4$ precipitation. Here, Cs$^+$ removal efficiency was surprisingly slightly lower compared to the kinetics study, owing to interaction with Ba^{2+} ions, while achieving superb Sr^{2+} removal in all cases. However, pretreatment of clinoptilolite with NaCl improved the removal efficiency of Cs$^+$, due to increased exchangeable Na$^+$ ions, resulting in combined removal efficiencies of >95 % for Cs$^+$ and >99.9 % for Sr^{2+}.

Overall, these results prove that simultaneous removal of Cs$^+$ and Sr^{2+} ions can be achieved by combining clinoptilolite and BaSO$_4$ together in a batch system. The innovation of this study comprises twofold benefits; 1) specific volume reduction due to faster settling and high-degree dewatering, which eases waste processing in solid encapsulation for long-term storage, and 2) enhanced simultaneous removal of Cs$^+$ and Sr^{2+} ions without the requirement for further ion exchange columns, which reduces the operational complexity, plant footprint, and operational costs. Further work is planned to determine the performance of the combined system in an intensified treatment process.

CRediT authorship contribution statement

Oguzhan Kivan: Writing – review & editing, Writing – original draft, Visualization, Validation, Project administration, Methodology, Investigation, Funding acquisition, Formal analysis, Conceptualization. **Muhammad Yusuf:** Writing – review & editing, Validation, Supervision, Conceptualization. **David Harbottle:** Writing – review & editing, Supervision. **Timothy N. Hunter:** Writing – review & editing, Supervision, Resources, Project administration, Methodology, Funding acquisition, Conceptualization.

Declaration of competing interest

The authors declare the following financial interests/personal relationships which may be considered as potential competing interests: Timothy N. Hunter reports financial support was provided by Engineering and Physical Sciences Research Council. If there are other authors, they declare that they have no known competing financial interests or personal relationships that could have appeared to influence the work reported in this paper.

Data availability

The data of this study are openly available from the University of Leeds Data Repository at https://doi.org/10.5518/1465 [112].

Acknowledgments

Appendix A. Supplementary data

Supplementary data to this article can be found online at https://doi.org/10.1016/j.jwpe.2024.104934.

References

[1] X. Liu, J. Wang, Adsorptive removal of Sr2+ and Cs+ from aqueous solution by capacitive deionization, Environ. Sci. Pollut. R. 28 (3) (2021), https://doi.org/10.1007/s11356-020-10691-6.

[2] M. Mahima Kumar, K.A. Irshad, H. Jena, Removal of Cs+ and Sr2+ ions from simulated radioactive waste solutions using Zeolite-A synthesized from kaolin and their structural stability at high pressures, Microporous Mesoporous Mater. 312 (2021), https://doi.org/10.1016/j.micromeso.2020.110773.

[3] J. Wang, S. Zhuang, Y. Liu, Metal hexacyanoferrates-based adsorbents for cesium removal, Coord. Chem. Rev. 374 (2018), https://doi.org/10.1016/j.ccr.2018.07.014.

[4] S. Chen, J. Hu, J. Shi, M. Wang, Y. Guo, M. Li, J. Duo, T. Deng, Composite hydrogel particles encapsulated ammonium molybdophosphate for efficiently cesium selective removal and enrichment from wastewater, J. Hazard. Mater. 371 (2019), https://doi.org/10.1016/j.jhazmat.2019.03.047.

[5] B. Aguila, D. Banerjee, Z. Nie, Y. Shin, S. Ma, P.K. Thallapally, Selective removal of cesium and strontium using porous frameworks from high level nuclear waste, Chem. Commun. 52 (35) (2016), https://doi.org/10.1039/C6CC00843G.

[6] N. Vajda, C.K. Kim, Determination of radiostrontium isotopes: a review of analytical methodology, Appl. Radiat. Isot. 68 (12) (2010), https://doi.org/10.1016/j.apradiso.2010.05.013.

[7] S. Chegrouche, A. Mellah, M. Barkat, Removal of strontium from aqueous solutions by adsorption onto activated carbon: kinetic and thermodynamic studies, Desalination 235 (1) (2009), https://doi.org/10.1016/j.desal.2008.01.018.

[8] X. Zhang, P. Gu, Y. Liu, Decontamination of radioactive wastewater: state of the art and challenges forward, Chemosphere (2019) 215, https://doi.org/10.1016/j.chemosphere.2018.10.029.

[9] S. İnan, Inorganic ion exchangers for strontium removal from radioactive waste: a review, J. Radioanal. Nucl. Chem. 331 (3) (2022), https://doi.org/10.1007/s10967-022-08206-3.

[10] Guidelines for Drinking-water Quality: Fourth Edition Incorporating the First and Second Addenda, World Health Organization, 2022.

[11] Radionuclides in Drinking Water: A Small Entity Compliance Guide, Environmental Protection Agency, 2002.

[12] Groundwater Monitoring at Sellafield: Annual Data Review, Sellafield Ltd., 2016.

[13] D.A. Bakhotmah, M.A. Hussein, W. El-Said, M.H. Ismael, E. Elshehy, Efficient removal of cesium and strontium from an aqueous solution using a zirconosilicate/vanadium oxide nanocomposite, J. Dispers. Sci. Technol. 44 (10) (2022), https://doi.org/10.1080/01932691.2022.2048005.

[14] A. Baeza, M. Fernández, M. Herranz, F. Legarda, C. Miró, A. Salas, Elimination of man-made radionuclides from natural waters by applying a standard coagulation-flocculation process, J. Radioanal. Nucl. Chem. 260 (2004), https://doi.org/10.1023/B:JRNC.0000027104.99292.6b.

[15] A.J. O'Donnell, D.A. Lytle, S. Harmon, K. Vu, H. Chait, D.D. Dionysiou, Removal of strontium from drinking water by conventional treatment and lime softening in bench-scale studies, Water Res. 103 (2016), https://doi.org/10.1016/j.watres.2016.06.036.

[16] H.A. Ibrahim, H.S. Hassan, H.S. Mekhamer, S.H. Kenawy, Diffusion and sorption of Cs+ and Sr2+ ions onto synthetic mullite powder, J. Radioanal. Nucl. Chem. 319 (1) (2019), https://doi.org/10.1007/s10967-018-6322-2.

[17] Y. Nishiyama, T. Hanafusa, J. Yamashita, Y. Yamamoto, T. Ono, Adsorption and removal of strontium in aqueous solution by synthetic hydroxyapatite, J. Radioanal. Nucl. Chem. 307 (2) (2016), https://doi.org/10.1007/s10967-015-4228-9.

[18] A. Dyer, et al., The use of columns of the zeolite clinoptilolite in the remediation of aqueous nuclear waste streams, J. Radioanal. Nucl. Chem. 318 (3) (2018), https://doi.org/10.1007/s10967-018-6329-8.

[19] G.M. Rashad, M.R. Mahmoud, M.A. Soliman, Combination of coprecipitation and foam separation processes for rapid recovery and preconcentration of cesium radionuclides from water systems, Process Saf. Environ. 130 (2019), https://doi.org/10.1016/j.psep.2019.08.007.

[20] A. Zhang, Q. Hu, Removal of cesium by countercurrent solvent extraction with a calix [4] crown derivative, Sep. Sci. Technol. 52 (10) (2017), https://doi.org/10.1080/01496395.2017.1297456.

[21] X. Liu, J. Wu, J. Wang, Removal of Cs (I) from simulated radioactive wastewater by three forward osmosis membranes, Chem. Eng. J. 344 (2018), https://doi.org/10.1016/j.cej.2018.03.046.

[22] Z.V.P. Murthy, S. Parmar, Removal of strontium by electrocoagulation using stainless steel and aluminum electrodes, Desalination 282 (2011), https://doi.org/10.1016/j.desal.2011.08.058.

[23] Y. Hu, X. Guo, C. Chen, J. Wang, Algal sorbent derived from Sargassum horneri for adsorption of cesium and strontium ions: equilibrium, kinetics, and mass transfer, Appl. Microbiol. Biotechnol. 103 (6) (2019), https://doi.org/10.1007/s00253-019-09619-z.

[24] L.H.V. Thanh, J.C. Liu, Flotation separation of strontium via phosphate precipitation, Water Sci. Technol. (2017), https://doi.org/10.2166/wst.2017.129, 75 (11-12).

[25] A.A. Alsarayreh, T.K. Abbas, S.O. Alaswad, S. e-Gul, A.D. Bajoga, Remove liquid radioactive wastes utilizing nanofiltration, ultrafiltration, and microfiltration membranes, Eng. Technol. J. 40 (9) (2022), https://doi.org/10.30684/etj.2022.134025.1218.

[26] H. Ma, H. Shen, Y. Tong, X. Wang, Radioactive wastewater treatment technologies: a review, Molecules 28 (4) (2023), https://doi.org/10.3390/molecules28041935.

[27] I. Smičiklas, S. Dimović, I. Plećaš, Removal of Cs1+, Sr2+ and Co2+ from aqueous solutions by adsorption on natural clinoptilolite, Appl. Clay Sci. 35 (1) (2007), https://doi.org/10.1016/j.clay.2006.08.004.

[28] M. Howden, Radioactive effluent treatment plant—sellafield reprocessing factory, P. I. Mech. Eng. A-J. Pow. 201 (1) (1987), https://doi.org/10.1243/PIME_PROC_1987_201_00.

[29] A. Dyer, in Introduction to Zeolite Science and Practice, Volume 168 (3rd Edition), Elsevier, 2007.

[30] R. Cortés-Martínez, M.T. Olguín, M. Solache-Ríos, Cesium sorption by clinoptilolite-rich tuffs in batch and fixed-bed systems, Desalination 258 (1) (2010), https://doi.org/10.1016/j.desal.2010.03.019.

[31] L. Al-Attar, A. Dyer, R. Harjula, Uptake of radionuclides on microporous and layered ion exchange materials, J. Mater. Chem. 13 (12) (2003), https://doi.org/10.1039/B308200H.

[32] B.R. Figueiredo, S.P. Cardoso, I. Portugal, J. Rocha, C.M. Silva, Inorganic ion exchangers for cesium removal from radioactive wastewater, Sep. Purif. Rev. 47 (4) (2018), https://doi.org/10.1080/15422119.2017.1392974.

[33] J. Wang, S. Zhuang, Removal of cesium ions from aqueous solutions using various separation technologies, Rev. Environ. Sci. Bio. 18 (2) (2019), https://doi.org/10.1007/s11157-019-09499-9.

[34] Y. Liu, P. Gu, L. Jia, G. Zhang, An investigation into the use of cuprous chloride for the removal of radioactive iodide from aqueous solutions, J. Hazard. Mater. 302 (2016), https://doi.org/10.1016/j.jhazmat.2015.09.045.

[35] G. Yaghy, et al., Opportunities for process intensification technologies in nuclear effluent treatment: a review of precipitators, adsorbers and separators, Chem. Eng. Process. 191 (2023), https://doi.org/10.1016/j.cep.2023.109441.

[36] T.A. Nedobukh, V.S. Semenishchev, Strontium: source, occurrence, properties, and detection, in: P. Pathak, D.K. Gupta (Eds.), Strontium Contamination in the Environment, Springer International Publishing, Cham, 2020.

[37] J.C. Fanning, The solubilities of the alkali metal salts and the precipitation of Cs+ from aqueous solution, Coord. Chem. Rev. 140 (1995), https://doi.org/10.1016/0010-8545(94)01123-S.

[38] M.A. Soliman, G.M. Rashad, M.R. Mahmoud, Fast and efficient cesium removal from simulated radioactive liquid waste by an isotope dilution–precipitate flotation process, Chem. Eng. J. 275 (2015), https://doi.org/10.1016/j.cej.2015.03.136.

[39] M. Oh, K. Lee, M.K. Jeon, R.I. Foster, C.-H. Lee, Chemical precipitation–based treatment of acidic wastewater generated by chemical decontamination of radioactive concrete, J. Environ. Chem. Eng. 11 (5) (2023), https://doi.org/10.1016/j.jece.2023.110306.

[40] X. Yang, L. Jiang, S. Peng, L. Zhang, G. Huang, Removal of cesium from liquid radioactive waste by in situ electrochemical synthesis of cesium zinc ferrocyanide, Colloids Surf. A Physicochem. Eng. Asp. 626 (2021), https://doi.org/10.1016/j.colsurfa.2021.127050.

[41] J.-G. Cao, P. Gu, J. Zhao, D. Zhang, Y. Deng, Removal of strontium from an aqueous solution using co-precipitation followed by microfiltration (CPMF), J. Radioanal. Nucl. Chem. 285 (3) (2010), https://doi.org/10.1007/s10967-010-0564-y.

[42] J. Lehto, R. Koivula, H. Leinonen, E. Tusa, R. Harjula, Removal of radionuclides from Fukushima Daiichi waste effluents, Sep. Purif. Rev. 48 (2) (2019), https://doi.org/10.1080/15422119.2018.1549567.

[43] K. Tokunaga, Y. Takahashi, K. Tanaka, N. Kozai, Effective removal of iodate by coprecipitation with barite: behavior and mechanism, Chemosphere (2021) 266, https://doi.org/10.1016/j.chemosphere.2020.129104.

[44] K. Shakir, H.F. Ghoneimy, S.G. Beheir, M. Refaat, Flotation of cesium coprecipitated with nickel hexacyanoferrate (II) from aqueous solutions and radioactive waste simulants, Sep. Sci. Technol. 42 (6) (2007), https://doi.org/10.1080/01496390601174257.

[45] J. Flouret, Y. Barré, H. Muhr, E. Plasari, Design of an intensified coprecipitation reactor for the treatment of liquid radioactive wastes, Chem. Eng. Sci. 77 (2012), https://doi.org/10.1016/j.ces.2012.01.051.

[46] J. Weber, et al., Unraveling the effects of strontium incorporation on barite growth—in situ and ex situ observations using multiscale chemical imaging, Cryst. Growth Des. 18 (9) (2018), https://doi.org/10.1021/acs.cgd.8b00839.

[47] H.A. Hunter, F.T. Ling, C.A. Peters, Metals coprecipitation with barite: nano-XRF observation of enhanced strontium incorporation, Environ. Eng. Sci. 37 (4) (2020), https://doi.org/10.1089/ees.2019.0447.

[48] C. YuHang, A. Asenjo, N. Sánchez-Pastor, L. Fernández-Díaz, J. Gómez, C.M. Pina, Growth of Bax Sr1−xSO4 nano-steps on barite (001) face, Surf. Sci. 601 (2) (2007), https://doi.org/10.1016/j.susc.2006.10.003.

[49] A.S. Tonge, D. Harbottle, S. Casarin, M. Zervaki, C. Careme, T.N. Hunter, Coagulated mineral adsorbents for dye removal, and their process intensification using an agitated tubular reactor (ATR), Chem. Eng. 5 (3) (2021), https://doi.org/10.3390/chemengineering5030035.

[50] J.-W. Lee, S.-P. Choi, R. Thiruvenkatachari, W.-G. Shim, H. Moon, Evaluation of the performance of adsorption and coagulation processes for the maximum removal of reactive dyes, Dyes Pigments 69 (3) (2006), https://doi.org/10.1016/j.dyepig.2005.03.008.

[51] F. Bu, B. Gao, Q. Yue, C. Liu, W. Wang, X. Shen, The combination of coagulation and adsorption for controlling ultra-filtration membrane fouling in water treatment, Water 11 (1) (2019), https://doi.org/10.3390/w11010090.

[52] H.-N. Kim, J.-H. Kim, I. Kim, I.-H. Yoon, Magnetic flocculants and selective adsorbents for the decontamination of radioactive and acidic soil-washing effluent, J. Water Process. Eng. 54 (2023), https://doi.org/10.1016/j.jwpe.2023.103964.

[53] M.Y. Prajitno, D. Harbottle, N. Hondow, H. Zhang, T.N. Hunter, The effect of pre-activation and milling on improving natural clinoptilolite for ion exchange of cesium and strontium, J. Environ. Chem. Eng. 8 (1) (2020), https://doi.org/10.1016/j.jece.2019.102991.

[54] V. Pacary, Y. Barré, E. Plasari, Method for the prediction of nuclear waste solution decontamination by coprecipitation of strontium ions with barium sulphate using the experimental data obtained in non-radioactive environment, Chem. Eng. Res. Des. 88 (9) (2010), https://doi.org/10.1016/j.cherd.2010.01.006.

[55] M.B. Rachida Otsmane, Hacène Saibi, Study of coprecipitation of strontium (Sr2+) with barium sulphate (BaSO4) in aqueous solution, J. Mater. Sci. Eng., A 5 (2015) 7–8, https://doi.org/10.17265/2161-6213/2015.7-8.006.

[56] E.H. Borai, R. Harjula, L. Malinen, A. Paajanen, Efficient removal of cesium from low-level radioactive liquid waste using natural and impregnated zeolite minerals, J. Hazard. Mater. 172 (1) (2009), https://doi.org/10.1016/j.jhazmat.2009.07.033.

[57] J. Chorover, S. Choi, M.K. Amistadi, K.G. Karthikeyan, G. Crosson, K.T. Mueller, Linking cesium and strontium uptake to kaolinite weathering in simulated tank waste leachate, Environ. Sci. Technol. 37 (10) (2003), https://doi.org/10.1021/es025980x.

[58] D.A. De Haro-Del Rio, S. Al-Joubori, O. Kontogiannis, D. Papadatos-Gigantes, O. Ajayi, C. Li, S.M. Holmes, The removal of caesium ions using supported clinoptilolite, J. Hazard. Mater. 289 (2015), https://doi.org/10.1016/j.jhazmat.2015.02.032.

[59] S. Azizian, Kinetic models of sorption: a theoretical analysis, J. Colloid Interface Sci. 276 (1) (2004), https://doi.org/10.1016/j.jcis.2004.03.048.

[60] R. Buscall, L.R. White, The consolidation of concentrated suspensions. Part 1.—the theory of sedimentation, J. Chem. Soc., Faraday Trans. I: Physical Chemistry in Condensed Phases 83 (3) (1987), https://doi.org/10.1039/F19878300873.

[61] M.D. Green, M. Eberl, K.A. Landman, Compressive yield stress of flocculated suspensions: determination via experiment, AIChE J 42 (8) (1996), https://doi.org/10.1002/aic.690420820.

[62] H.N. Yow, S. Biggs, Probing the stability of sterically stabilized polystyrene particles by centrifugal sedimentation, Soft Matter 9 (42) (2013), https://doi.org/10.1039/C3SM51534F.

[63] E. Höfgen, H.-E. Teo, P.J. Scales, A.D. Stickland, Vane-in-a-filter and vane-under-compressional-loading: novel methods for the characterisation of combined shear and compression, Rheol. Acta 59 (6) (2020), https://doi.org/10.1007/s00397-020-01193-w.

[64] G. Carotenuto, Electrical investigation of the mechanism of water adsorption/desorption by natural clinoptilolite desiccant used in food preservation, Mater. Proc. 2 (1) (2020), https://doi.org/10.3390/CIWC2020-06800.

[65] N. Mansouri, N. Rikhtegar, H. Panahi, F. Atabi, B. Karimi Shahraki, Porosity, characterization and structural properties of natural zeolite - Clinoptilolite-as a sorbent, Environ. Prot. Eng. 39 (2013), https://doi.org/10.5277/EPE130111.

[66] V. Ramaswamy, R.M. Vimalathithan, V. Ponnusamy, Synthesis and characterization of BaSO4 Nano-particles using micro-emulsion technique, Adv. Appl. Sci. Res. 1 (3) (2010) 197–204.

[67] E.D. Bolaina-Lorenzo, J.M. Cervantes-Uc, J.V. Cauich-Rodriguez, A. Avila-Ortega, J.A. Juarez-Moreno, Effect of barium sulfate surface treatments on the mechanical properties of acrylic bone cements, Polym. Bull. 78 (10) (2021), https://doi.org/10.1007/s00289-020-03407-w.

[68] A. Saravanan, P. Senthil Kumar, S. Jeevanantham, S. Karishma, B. Tajsabreen, P. R. Yaashikaa, B. Reshma, Effective water/wastewater treatment methodologies for toxic pollutants removal: processes and applications towards sustainable development, Chemosphere 280 (2021), https://doi.org/10.1016/j.chemosphere.2021.130595.

[69] M.S. Nasser, A.E. James, The effect of polyacrylamide charge density and molecular weight on the flocculation and sedimentation behaviour of kaolinite suspensions, Sep. Purif. Technol. 52 (2) (2006), https://doi.org/10.1016/j.seppur.2006.04.005.

[70] J. Mähler, I. Persson, A study of the hydration of the alkali metal ions in aqueous solution, Inorg. Chem. 51 (1) (2012), https://doi.org/10.1021/ic2018693.

[71] S. Amanipour, H. Faghihian, Potassium hexacyanoferrate–clinoptilolite adsorbent for removal of Cs+ and Sr2+ from aqueous solutions, Int. J. Environ. Stud. 74 (1) (2017), https://doi.org/10.1080/00207233.2016.1245063.

[72] K. Nemoto, N. Nihei, Transfer of radiocesium to rice in contaminated paddy fields, in: T.M. Nakanishi, M. O'Brien, K. Tanoi (Eds.), Agricultural Implications of the Fukushima Nuclear Accident (III): After 7 Years, Springer Singapore, 2019, pp. 9–14.

[73] E. Akyol, M.A. Cedimagar, Size and morphology controlled synthesis of barium sulfate, Cryst. Res. Technol. 51 (6) (2016), https://doi.org/10.1002/crat.201600046.

[74] M.A. Hernandez, et al., CO2 adsorption on natural zeolites from Puebla, Mexico, by inverse gas chromatography, Separations 10 (4) (2023), https://doi.org/10.3390/separations10040238.

[75] M. Pieper, S. Aman, J. Tomas, Agglomeration kinetics of submicron barium sulfate precipitates, Chem. Eng. Sci. 77 (2012), https://doi.org/10.1016/j.ces.2011.12.043.

[76] A.P.G. Lockwood, J. Peakall, N.J. Warren, G. Randall, M. Barnes, D. Harbottle, T. N. Hunter, Structure and sedimentation characterisation of sheared Mg (OH)2 suspensions flocculated with anionic polymers, Chem. Eng. Sci. (2021) 231, https://doi.org/10.1016/j.ces.2020.116274.

[77] D. Jana, A New Look to an Old Pozzolan: Clinoptilolite - A Promising Pozzolan in Concrete, in International Cement Microscopy Association -29th International Conference on Cement Microscopy, 2007.

[78] M.Y. Prajitno, S. Tangparitkul, H. Zhang, D. Harbottle, T.N. Hunter, The effect of cationic surfactants on improving natural clinoptilolite for the flotation of cesium, J. Hazard. Mater. 402 (2021), https://doi.org/10.1016/j.jhazmat.2020.123567.

[79] P. Kowalczyk, M. Sprynskyy, A.P. Terzyk, M. Lebedynets, J. Namieśnik, B. Buszewski, Porous structure of natural and modified clinoptilolites, J. Colloid Interface Sci. 297 (1) (2006), https://doi.org/10.1016/j.jcis.2005.10.045.

[80] J. Hang, L. Shi, X. Feng, L. Xiao, Electrostatic and electrosteric stabilization of aqueous suspensions of barite nanoparticles, Powder Technol. 192 (2) (2009), https://doi.org/10.1016/j.powtec.2008.12.010.

[81] M. Zhang, B. Zhang, X. Li, Z. Yin, X. Guo, Synthesis and surface properties of submicron barium sulfate particles, Appl. Surf. Sci. 258 (1) (2011), https://doi.org/10.1016/j.apsusc.2011.07.137.

[82] J.N. Bracco, et al., Simultaneous adsorption and incorporation of Sr2+ at the Barite (001)–water interface, J. Phys. Chem. C 123 (2) (2019), https://doi.org/10.1021/acs.jpcc.8b08848.

[83] Z. Peng, J. Wen, Y. Liu, G. Zeng, Y. Yi, Y. Fang, S. Zhang, J. Deng, X. Cai, Heavy metal leachability in soil amended with zeolite- or biochar-modified contaminated sediment, Environ. Monit. Assess. 190 (12) (2018), https://doi.org/10.1007/s10661-018-7124-2.

[84] S.V. Sujith, H. Kim, J. Lee, A review on thermophysical property assessment of metal oxide-based nanofluids: industrial perspectives, Metals 12 (1) (2022), https://doi.org/10.3390/met12010165.

[85] W. Francis, M.C. Peters, Data sheet no. 11- coal preparation—mechanical cleaning—theory, in: W. Francis, M.C. Peters (Eds.), Fuels and Fuel Technology, Second edition, 1980, pp. 59–64. Pergamon.

[86] M. Johnson, J. Peakall, M. Fairweather, S. Biggs, D. Harbottle, T.N. Hunter, Characterization of multiple hindered settling regimes in aggregated mineral suspensions, Ind. Eng. Chem. Res. 55 (37) (2016), https://doi.org/10.1021/acs.iecr.6b02383.

[87] A.D. Stickland, C. Burgess, D.R. Dixon, P.J. Harbour, P.J. Scales, L.J. Studer, S.P. Usher, Fundamental dewatering properties of wastewater treatment sludges from filtration and sedimentation testing, Chem. Eng. Sci. 63 (21) (2008), https://doi.org/10.1016/j.ces.2008.07.016.

[88] Y.S. Ho, G. McKay, Pseudo-second order model for sorption processes, Process Biochem. 34 (5) (1999), https://doi.org/10.1016/S0032-9592(98)00112-5.

[89] N. Gupta, R. Sen, Kinetic and equilibrium modelling of Cu (II) adsorption from aqueous solution by chemically modified Groundnut husk (Arachis hypogaea), J. Environ. Chem. Eng. 5 (5) (2017), https://doi.org/10.1016/j.jece.2017.07.048.

[90] H. Zhang, L. Gu, L. Zhang, S. Zheng, H. Wan, J. Sun, D. Zhu, Z. Xu, Removal of aqueous Pb (II) by adsorption on Al2O3-pillared layered MnO2, Appl. Surf. Sci. 406 (2017), https://doi.org/10.1016/j.apsusc.2017.02.011.

[91] N. Lihareva, O. Petrov, L. Dimowa, Y. Tzvetanova, I. Piroeva, F. Ublekov, A. Nikolov, Ion exchange of Cs+ and Sr2+ by natural clinoptilolite from bi-cationic solutions and XRD control of their structural positioning, J. Radioanal. Nucl. Chem. 323 (3) (2020), https://doi.org/10.1007/s10967-020-07018-7.

[92] S. Kwon, C. Kim, E. Han, H. Lee, H.S. Cho, M. Choi, Relationship between zeolite structure and capture capability for radioactive cesium and strontium, J. Hazard. Mater. 408 (2021), https://doi.org/10.1016/j.jhazmat.2020.124419.

[93] M. Şenilä, E. Neag, C. Tănăselia, L. Şenilă, Removal of cesium and strontium ions from aqueous solutions by thermally treated natural zeolite, Materials 16 (8) (2023), https://doi.org/10.3390/ma16082965.

[94] K. Tokunaga, N. Kozai, Y. Takahashi, A new technique for removing strontium from seawater by coprecipitation with barite, J. Hazard. Mater. 359 (2018), https://doi.org/10.1016/j.jhazmat.2018.07.044.

[95] L. Lumiste, S. Ponnusamy, R. Munter, S. Deng, 266034 Removal of Barium From Ground Water Using Clinoptilolite, in 12 AIChE Annual Meeting, 2012.

[96] M. Dosa, M. Piumetti, S. Bensaid, N. Russo, O. Baglieri, F. Miglietta, D. Fino, Properties of the Clinoptilolite: characterization and adsorption tests with methylene blue, J. Adv. Catal. Sci. Techno. (2018), https://doi.org/10.15379/2408-9834.2018.05.01.01.

[97] F.A. Mumpton, La roca magica: uses of natural zeolites in agriculture and industry, Proc. Natl. Acad. Sci. U. S. A. 96 (7) (1999), https://doi.org/10.1073/pnas.96.7.3463.

[98] A.E. Osmanlioglu, Treatment of radioactive liquid waste by sorption on natural zeolite in Turkey, J. Hazard. Mater. 137 (1) (2006), https://doi.org/10.1016/j.jhazmat.2006.02.013.

[99] S. Wang, Y. Peng, Natural zeolites as effective adsorbents in water and wastewater treatment, Chem. Eng. J. 156 (2) (2010), https://doi.org/10.1016/j.cej.2009.10.029.

[100] V.J. Inglezakis, The concept of "capacity" in zeolite ion-exchange systems, J. Colloid Interface Sci. 281 (1) (2005), https://doi.org/10.1016/j.jcis.2004.08.082.

[101] M.M. Motsa, B.B. Mamba, J.M. Thwala, T.A. Msagati, Preparation, characterization, and application of polypropylene-clinoptilolite composites for the selective adsorption of lead from aqueous media, J. Colloid Interface Sci. 359 (1) (2011), https://doi.org/10.1016/j.jcis.2011.02.067.

[102] S. Eun, J. Ryu, H. Kim, H.-J. Hong, S. Kim, Simultaneous removal of radioactive cesium and strontium from seawater using a highly efficient Prussian blue-embedded alginate aerogel, J. Environ. Manage. 297 (2021), https://doi.org/10.1016/j.jenvman.2021.113389.

[103] S.S. Metwally, I.M. Ahmed, H.E. Rizk, Modification of hydroxyapatite for removal of cesium and strontium ions from aqueous solution, J. Alloys Compd. 709 (2017), https://doi.org/10.1016/j.jallcom.2017.03.156.

[104] A.R. Khanchi, R. Yavari, S.K. Pourazarsa, Preparation and evaluation of composite ion-exchanger for the removal of cesium and strontium radioisotopes, J. Radioanal. Nucl. Chem. 273 (1) (2007), https://doi.org/10.1007/s10967-007-0725-9.

[105] T. Wen, Z. Zhao, C. Shen, J. Li, X. Tan, A. Zeb, X. Wang, A.-W. Xu, Multifunctional flexible free-standing titanate nanobelt membranes as efficient sorbents for the removal of radioactive 90Sr2+ and 137Cs+ ions and oils, Sci. Rep. 6 (1) (2016), https://doi.org/10.1038/srep20920.

[106] A.M. El-Kamash, M.R. El-Naggar, M.I. El-Dessouky, Immobilization of cesium and strontium radionuclides in zeolite-cement blends, J. Hazard. Mater. 136 (2) (2006), https://doi.org/10.1016/j.jhazmat.2005.12.020.

[107] J.H. Sharp, J. Hill, N.B. Milestone, E.W. Miller, Cementitious systems for encapsualation of intermediate level waste, in: ASME 2003 9th International Conference on Radioactive Waste Management and Environmental Remediation, 2003.

[108] C. Kuenzel, J.F. Cisneros, T.P. Neville, L.J. Vandeperre, S.J.R. Simons, J. Bensted, C.R. Cheeseman, Encapsulation of Cs/Sr contaminated clinoptilolite in geopolymers produced from metakaolin, J. Nucl. Mater. 466 (2015), https://doi.org/10.1016/j.jnucmat.2015.07.034.

[109] Y. Zhu, Z. Zheng, Y. Deng, C. Shi, Z. Zhang, Advances in immobilization of radionuclide wastes by alkali activated cement and related materials, Cem. Concr. Compos. 126 (2022), https://doi.org/10.1016/j.cemconcomp.2021.104377.

[110] J.M. Juoi, M.I. Ojovan, W.E. Lee, Microstructure and leaching durability of glass composite wasteforms for spent clinoptilolite immobilisation, J. Nucl. Mater. 372 (2) (2008), https://doi.org/10.1016/j.jnucmat.2007.04.047.

[111] O. Hussein, C. Utton, M. Ojovan, H. Kinoshita, The effects of BaSO4 loading on OPC cementing system for encapsulation of BaSO4 scale from oil and gas industry, J. Hazard. Mater. (2013) 261, https://doi.org/10.1016/j.jhazmat.2013.06.048.

[112] O. Kivan, M. Yusuf, D. Harbottle, T.N. Hunter, Removal of Cesium and Strontium Ions with Enhanced Solid-Liquid Separation by Combined Ion Exchange and BaSO4 Co-Precipitation - Dataset, 2024, https://doi.org/10.5518/1465.